J. Fluid Mech. (1999), *vol.* 380, *pp.* 339–361. Printed in the United Kingdom

The role of 'splashing' in the collapse of a laser-generated cavity near a rigid boundary

By R. P. TONG[1], W. P. SCHIFFERS[2], S. J. SHAW[3], J. R. BLAKE[1] AND D. C. EMMONY[2]

[1]School of Mathematics and Statistics, The University of Birmingham, Edgbaston, Birmingham, B15 2TT, UK

[2]Department of Physics, University of Loughborough, Loughborough, Leicestershire, LE11 3TU, UK

[3]Department of AAETS, University of Loughborough, Loughborough, Leicestershire, LE11 3TU, UK

(Received 3 June 1997 and in revised form 2 October 1998)

Vapour cavities in liquid flows have long been associated with cavitation damage to nearby solid surfaces and it is thought that the final stage of collapse, when a high-speed liquid jet threads the cavity, plays a vital role in this process. The present study investigates this aspect of the motion of laser-generated cavities in a quiescent liquid when the distance (or stand-off) of the point of inception from a rigid boundary is between 0.8 and 1.2 times the maximum radius of the cavity. Numerical simulations using a boundary integral method with an incompressible liquid impact model provide a framework for the interpretation of the experimental results. It is observed that, within the given interval of the stand-off parameter, the peak pressures measured on the boundary at the first collapse of a cavity attain a local minimum, while at the same time there is an increase in the duration of the pressure pulse. This contrasts with a monotonic increase in the peak pressures as the stand-off is reduced, when the cavity inception point is outside the stated interval. This phenomenon is shown to be due to a splash effect which follows the impact of the liquid jet. Three cases are chosen to typify the splash interaction with the free surface of the collapsing cavity: (i) surface reconnection around the liquid jet; (ii) splash impact at the base of the liquid jet; (iii) thin film splash. Hydrodynamic pressures generated following splash impact are found to be much greater than those produced by the jet impact. The combination of splash impact and the emission of shock waves, together with the subsequent re-expansion, drives the flow around the toroidal cavity producing a distinctive double pressure peak.

1. Introduction

The collapse of vapour cavities in a liquid, typically water, has been studied extensively in connection with the pitting and erosion which are observed in hydraulic machinery exposed to cavitating flows. The particular focus of this study is on the behaviour of single bubbles and it therefore also has relevance to bubbles produced by underwater explosions (Cole 1948) or in laser surgery (Vogel & Busch 1994). It has been known since the work of Rayleigh (1917) that, for a spherical vapour cavity, very high pressures are generated in the liquid close to the cavity surface during the final stages of collapse. However, more recently, attention has focused on the asymmetry

which is observed in a cavity collapsing near a rigid boundary (Benjamin & Ellis 1966). This asymmetry leads to the formation of a high-speed liquid jet which penetrates the cavity and which, in the absence of significant opposing buoyancy forces, is directed towards the boundary. The impact which results when the liquid jet meets the far surface of the cavity has been proposed as the main mechanism in cavitation damage. This complex process is still not fully understood and the present study examines the flow at jet impact and the subsequent formation of a toroidal cavity close to a rigid boundary. For a particular interval of the stand-off parameter, the flow associated with the toroidal cavity is found to produce hydrodynamic pressures on the adjacent boundary which are far higher than those associated with the initial jet impact.

The appearance of vapour cavities in a flow is facilitated by the presence of small pockets of undissolved gas already in the liquid which then form part of the cavity contents (Batchelor 1967). However, the final stage of collapse is so rapid that it exceeds the condensation rate of the vapour and, even in the case of cavities containing pure liquid vapour, internal pressures are generated which are sufficient to halt the contraction and initiate a re-expansion or rebound (Fujikawa & Akamatsu 1980). A typical cavity can thus be expected to undergo several oscillations during its lifetime.

In the laboratory, laser-generated cavities are used to study the effects of cavitation in a quiescent liquid under controlled conditions. This method of initiation leads to the production of additional non-condensable gaseous contents due to dissociation of the liquid molecules (water in this case) under the action of the laser. In a number of previous studies, laser pulses have been used to generate cavities in liquid, see for example, Lauterborn (1974), Vogel, Lauterborn & Timm (1989) or Ohl, Philipp & Lauterborn (1995). These have been useful in establishing some of the main features of cavity collapse near a rigid boundary such as the formation of the liquid jet, migration of the cavity over several oscillations, the emission of acoustic waves and the appearance of pitting damage on the boundary.

Shock waves are emitted by cavities of this type at the time of rebound and, in the case of laser-generated cavities, at the time of inception. However, shock waves alone are not thought to be sufficient to cause the marking and pitting damage to nearby rigid boundaries associated with cavitation. Shaw *et al.* (1996) report an experiment where a cavity is generated between two parallel planes 3 mm apart, the point of inception of the cavity being 1.3 mm from the nearest boundary. During collapse a jet penetrates the cavity in the direction of the nearer plane, accompanied by a migration of the cavity centroid towards this plane. The fact that damage is only evident on the nearer plane and that the shock pressures on both boundaries are similar is one indication that the flow induced by the collapsing cavity around the time of jet impact (which is directed towards the boundary) is likely to be a significant factor in the damage-causing mechanism.

The significant parameter is the non-dimensional stand-off, defined as the distance of the point of inception from the boundary scaled by the maximum cavity radius, which is denoted here by γ. Philipp & Lauterborn (1997) note the sensitivity of cavity collapse to the stand-off in their study of damage patterns for $\gamma = 1.5$–1.7. It is observed by Tomita & Shima (1986) that the peak pressures recorded on the boundary for a cavity of a given maximum radius increase monotonically as the location of cavity inception is moved closer, until $\gamma \approx 1.2$. These peak pressures are identified as due to the shock waves radiated as the cavity rebounds from minimum volume. However, this increase in pressures is interrupted as the cavity stand-off is further reduced. For $0.6 < \gamma < 1.2$, there is a fall in the peak pressures to a

local minimum followed by a resumption of the increasing trend for $\gamma < 0.6$. These observations are confirmed by Vogel & Lauterborn (1988), Vogel *et al.* (1989) and Philipp & Lauterborn (1998). The local minimum coincides with a maximum in the rise time of the pressure gauge, indicating that factors other than the shock waves are significant. Tomita & Shima (1986) further indicate that this interval of the parameter γ corresponds to cases where the effects of jet impact are felt at the rigid boundary before the cavity reaches minimum volume. For $\gamma < 1.0$, the impact of the axisymmetric liquid jet leads to a flow which spreads radially outwards from the jet axis along the boundary. The authors suggest that this radial flow is an important feature of cavities collapsing close to a boundary. They postulate that the pitting damage to nearby structures caused by cavity collapse is related to high-speed microjets produced by the interaction of the previously mentioned shock waves with very small bubbles formed by the breakup of the main cavity in the radial flow.

This paper focuses on the final stage of the first collapse, including jet impact and the transition to a toroidal cavity, for the stand-off parameter in the interval $0.8 \leqslant \gamma \leqslant 1.2$. This interval of the stand-off parameter includes the fall in the peak shock pressures to a local minimum mentioned above. Shaw *et al.* (1996) note that the pressure transducer readings for laser-generated cavities with $\gamma \approx 5/6$ and $\gamma \approx 1$ show a double peaked structure. For the case $\gamma \approx 5/6$, a short-duration pressure pulse is recorded approximately 15 μs after the jet has penetrated the cavity and is followed some 5 μs later by a second pressure peak. This is interpreted by the authors to be a shock-induced peak preceding a pressure peak of longer duration produced by flow through the torus. The combination of the two peaks would account for the longer gauge rise time reported by Tomita & Shima (1986). The numerical and experimental results of the present study show that the pressure data can be related to splashing in the flow which develops during the early stages of the toroidal cavity formed upon jet impact.

The nature of the impact on the region of the cavity surface closest to the rigid boundary is crucial to the determination of the resulting flow. The cases presented here involve liquid–liquid impact where there is a thin layer of liquid separating the cavity from the boundary at the moment of contact with the jet tip. Liquid impact has been the subject of extensive research and §2 reviews those aspects, such as splash formation, which are relevant to the present situation. Consideration of the impact process leads to the adoption of the numerical model proposed by Best (1993) which is outlined in §3. The results of the numerical simulations described in §4 illustrate the relationship between the flows following jet impact, the evolution of the cavity surface shapes and the pressures induced on the rigid boundary. In §5 the experimental method for laser-generated cavities is outlined and in §6 the experimental results for typical cases show how the thickness of the liquid layer between the collapsing cavity and the rigid plane influences the flow field, in confirmation of the numerical predictions.

2. The nature of liquid impact

The essential features of the jet impact must be identified in order to gain an understanding of the subsequent flow and to develop an appropriate numerical model. If the cavity is very close to the rigid boundary, then it is possible that any liquid separating the cavity from the boundary will be driven out as the cavity expands resulting in a jet impact directly onto the rigid plane. The liquid–solid impact which

arises in this case is not investigated in this paper, but attention is directed to impact of the jet onto a thin layer of liquid on the boundary. The experiments described below involve laser-generated cavities in water which expand to a maximum radius of 1.3 mm for values of the stand-off parameter $0.8 < \gamma < 1.2$. The impacts are of water jets approximately 0.2 mm in diameter travelling at velocities in the region of 100 m s^{-1}. This gives Weber numbers, $We = (\rho D V^2/\sigma)^{1/2} \approx 10^4$ and Froude numbers, $Fr = V/(gD)^{1/2} \approx 10^3$, so that the effects of surface tension, σ, and the acceleration due to gravity, g, on the motion are negligible. (Here D is the jet tip diameter at impact and V is the jet velocity.)

Since the interior of a collapsing cavity is not easily observed, there has been some speculation concerning the exact nature of the jet impact. Zhang, Duncan & Chahine (1993) suggest that a vortex sheet is formed which separates the jet from the surrounding liquid during the impact process. On the other hand, Best (1993) models the impact as an instantaneous event resulting in a circulation around the now toroidal cavity, but without the appearance of a vortex sheet. A contrasting numerical scheme for the motion of free surfaces, including the colliding surfaces which occur in cavity collapse, is presented in Rogers & Szymczak (1997). The free surface is not explicitly tracked in time, but the density is treated as a variable, subject to a constraint which ensures mass conservation. The method allows for energy losses as a result of liquid impacts. None of these approaches includes the compressible effects which are likely to be associated with the initial impact. It is argued here that there are clear physical criteria for determining those features of liquid–liquid impact which have a significant effect on the flow which subsequently develops. These arguments are confirmed by the experimental and numerical results and are consistent with earlier work (as discussed below) on liquid impact in other contexts. Findings for both liquid drop and jet impact are relevant since the initial impact is similar in both cases, as noted by Hand, Field & Townsend (1991).

The pitting damage observed on surfaces exposed to cavitating flows is similar to that caused by high-speed liquid jet or drop impact. However, experimental evidence (Bourne, Obara & Field 1997; Bowden & Brunton 1961) indicates that velocities in excess of 500 m s^{-1} are required for water jets 1–3 mm in diameter to produce noticeable damage on PMMA. For impacts at these velocities compressible effects are important, although short-lived, and can lead to additional complexities in the flow such as a cavitation cloud ahead of the jet following impact (Bourne, Obara & Field 1996). In the examples of cavity collapse discussed here, the much lower jet velocities suggest that the impacts are not in themselves capable of causing marking of the material of the rigid boundary as earlier noted by Tomita & Shima (1986).

Peak pressures of the order of the water hammer pressure of $\rho c V$ (where c is the speed of sound in the liquid) are expected to be generated by jet impact. These do not, however, appear in the pressure gauge output of the present experiments, nor of those reported by Tomita & Shima (1986). This can be explained by the fact that the jet diameter is much smaller than that of the pressure transducer and also that these peak pressures are very short-lived. Impact onto a liquid layer can reduce the pressures registered on the rigid boundary, yet in the experiments of Johnson & Vickers (1973) the peak pressures from jet impact onto a thin liquid film were of the same magnitude as for impact onto a dry surface. The time interval for which large pressures due to compressible effects are likely to exist can be estimated for a jet bounded by a smooth, typically hemispherical, surface (Lesser 1981; Guo & Ffowcs Williams 1991). In terms of the Mach number, $M \ll 1$, the duration time $\sim M^2 D/V$, where D is the jet diameter. For the experimental results of the present study, this

is only a few nanoseconds while the period of the first cavity oscillation cycle lasts approximately 250 μs.

Korobkin (1997) divides liquid impact into five stages for the purpose of obtaining asymptotic solutions: supersonic stage; transonic stage; subsonic stage; inertia stage; stage of developed liquid flow. During the first four stages the liquid flow and deformations of the free surface can be neglected outside a small region containing the line of contact of the liquid jet. In the present study attention is directed to the evolution of the cavity free surface through the collapse and into the toroidal stage of motion. The impact is thus viewed as consisting of two stages: an initial compressible stage which is too short-lived to produce significant deformation of the free surface; second, a stage of developed flow where the liquid can be regarded as incompressible. This suggests that a mathematical formulation following the free surface motion can ignore compressible effects which do not influence the subsequent flow.

Such a view is consistent with the argument of Yarin & Weiss (1995) that compressible effects are 'forgotten' almost instantaneously on the time scale of the process of splashing during liquid drop impact onto a solid plane. This is confirmed by their experimental results which indicate that drop diameter does not correlate with the surface motion. The similarity between the evolution of 3.5 mm radius spark-generated cavities reported by Tomita & Shima (1986) and the 1.3 mm radius laser-generated cavities of the present experiments, with a corresponding difference in the radii of the liquid jets, is one indication that compressible effects are not important in determining the flow which follows jet impact for the examples of collapsing cavities considered in this paper. A similar argument based on time scales is used by Oğuz & Prosperetti (1989) to justify their formulation of the free surface motion of a raindrop falling onto water as being an incompressible flow, while Howison, Ockendon & Wilson (1991) derive an incompressible model to describe solid–liquid impact.

The characteristics of the flow after jet impact onto the layer of liquid separating the cavity from the boundary is difficult to determine from experimental observation. However, it is possible to use the evidence of studies of liquid drop and jet impact onto a quiescent liquid layer in other contexts to shed light on this. The important features which need to be considered are the possible generation of vorticity and the conditions which lead to the formation of a splash. The term 'splash' is generally used to refer to the projection from the main liquid body of a thin liquid film which breaks up into small drops at its edge or rim. For the present discussion, the term 'splash' is taken to refer to an annulus of liquid which is projected from the liquid layer around the jet, following impact. This is in a direction opposite to that of the jet and, since this occurs within the confines of the closed surface of a cavity, its breakup into droplets is likely to be restricted.

Cresswell & Morton (1995) present an analysis of experiments of drop impact, arguing that a vortex sheet enveloping the drop liquid is not produced by impacts at high velocities. The formation of a vortex ring due to the separation of the vortex sheet generated at the ring of contact between the drop and liquid layer when surface tension effects are important is found to occur for $We < 8$. Further experiments for water drop impact onto water are described by Rein (1996). These show that, as the Weber number increases, there is a transition from drop coalescence (accompanied by the generation of vorticity and the formation of a vortex ring) to splashing. A dependence of the Weber number on the Froude number is also demonstrated. It is shown that a splash is produced by the impact of a drop of radius 2.5 mm at a velocity of 5 m s^{-1} with $We \approx 42$ and $Fr \approx 22$. A quasi-one-dimensional theoretical model of the splashing of a train of liquid drops impinging on a solid plane is used by

Yarin & Weiss (1995) to explain their experimental data. Compressibility and viscous effects are ignored, along with gravity and surface tension, to arrive at a solution for depth-averaged flow in the thin film produced by the drop impacts. This solution possesses a discontinuity when there is a negative gradient in the spatial derivative of the initial velocity distribution with respect to distance from the location of the drop impact. The discontinuity condition is satisfied by an outwardly propagating sink which represents the splash.

After impact, an impinging jet drives a flow which spreads radially outwards along the rigid boundary from the jet axis leading to the outward propagation and rise of a splash film. The liquid accelerations at the base of the splash, as a result of this flow, can be expected to produce an expanding ring of higher pressure on the boundary. If this flow were to be contained within a cylindrical solid boundary perpendicular to the plane on which the jet impact occurs, then an axisymmetric filling flow as defined by Peregrine & Kalliadasis (1996) would result. In this latter situation the maximum pressures occur on the sides of the cylindrical boundary at locations which are stagnation points in a frame in which the free surface is stationary. These peak pressures can be several times larger than the stagnation point pressure of $\rho V^2/2$ which would be generated on the axis of symmetry for the steady flow of an incompressible impinging jet. In the case of the propagating splash, it is therefore expected that an annulus of high pressure will travel with the splash, surrounding the impinging jet.

For liquid jet impact on a deep liquid layer the initial splash may be followed by reconnection of the free surface of the main body of liquid to the incoming jet surface. This can lead to the entrainment of small bubbles and the generation of turbulence. This type of flow has been investigated by Oğuz, Prosperetti & Kolaini (1995) in connection with bubble formation following the impact of a liquid slug. It has some similarities with the reconnection of the cavity formed behind a solid sphere after an impact into a deep liquid layer (Gilbarg & Anderson 1948).

The parameters stated for the examples of cavity collapse that are discussed in this paper place the jet impacts well within the splashing flow regime. The following sections show how the splashing phenomenon interacts with the collapsing cavity to produce particular flow effects which can be simulated numerically and which are confirmed by experiment.

3. Mathematical model

In view of the discussion of the preceding section, it is possible to specify the essential features of the jet impact and subsequent flow for a cavity collapsing near a rigid boundary. Compressible effects associated with the jet impact are ignored since the focus is on the free surface motion over the period of cavity expansion and collapse. The liquid–liquid impacts are not considered to produce significant vorticity, a fact which is confirmed by the experimental evidence outlined in the previous section, and it is therefore not necessary to model the formation of a vortex sheet. The significant feature of the impacts which must be modelled is the circular liquid splash film which is projected away from the boundary. This propagates outward from the impact site along the boundary, carried by the radial flow due to the impinging jet. Although the impact does not produce vorticity, it does lead to a circulation around the toroidal shaped cavity which is formed.

The liquid containing the cavity is therefore assumed to be incompressible and irrotational, while the effects of gravity, surface tension and viscosity are ignored.

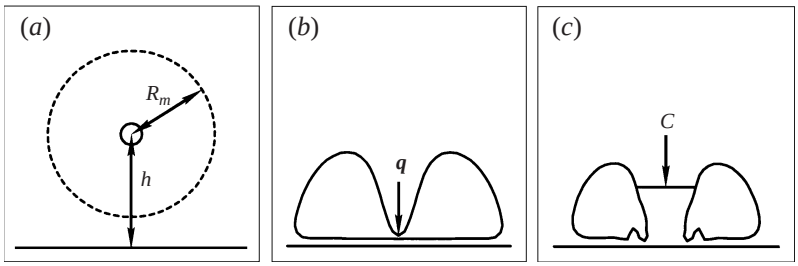

FIGURE 1. (*a*) Location of the cavity in relation to the rigid boundary. R_m is the radius at maximum expansion, giving $\gamma = h/R_m$. (*b*) The point of jet impact, $\boldsymbol{q}$. (*c*) The toroidal cavity showing the cut C which is introduced to define a simply-connected computational domain.

The motion can thus be described by a velocity potential $\phi(\boldsymbol{x}, t)$ (where $\boldsymbol{x}$ denotes position with respect to Cartesian coordinates) which satisfies Laplace's equation in a semi-infinite domain, Ω, bounded by the free surface of the cavity and the rigid plane boundary (see figure 1*a*). In addition to the liquid vapour, the pressure inside the cavity includes a contribution due to non-condensable gas, which is likely to originate as a result of dissociation caused by the initial laser pulse. A simple adiabatic model is used for the variation of cavity pressure, p_c, giving

$$p_c = p_v + p_0 \left(\frac{V_0}{V} \right)^{\kappa}, \tag{3.1}$$

where p_v is the vapour pressure, p_0 is the pressure of the non-condensable contents near the time of cavity inception when the volume is V_0, and κ is the ratio of specific heats.

The following scalings are chosen: lengths by R_m, the maximum radius attained by a spherical bubble in an infinite domain for the given initial conditions; pressure by $\Delta p = p_\infty - p_v$, where p_∞ is the ambient pressure at the location of cavity inception; time by $R_m(\rho/\Delta p)^{1/2}$; potential by $R_m(\Delta p/\rho)^{1/2}$. The governing equations are then

$$\nabla^2 \phi = 0 \qquad \text{in} \quad \Omega, \tag{3.2}$$

with the free surface boundary conditions

$$\frac{\mathrm{D}\phi}{\mathrm{D}t} = \frac{1}{2}|\nabla\phi|^2 - \alpha \left(\frac{V_0}{V} \right)^{\kappa} + 1, \tag{3.3}$$

where $\alpha = p_0/\Delta p$ and

$$\frac{\mathrm{D}\boldsymbol{x}}{\mathrm{D}t} = \nabla\phi, \tag{3.4}$$

while on the rigid boundary

$$\frac{\partial\phi}{\partial n} = 0. \tag{3.5}$$

With these assumptions, incompressible jet impact can be regarded as an impulsive fluid motion of the type described by Batchelor (1967), where the magnitudes of the liquid velocity and its spatial derivatives are very much smaller than the time derivative of the velocity over the short time of the impulse. Since the conditions for the Kelvin circulation theorem are satisfied, the irrotational motion prior to impact remains irrotational after impact. This defines the change in potential over the time

of the impact as

$$\phi'' - \phi' = -\frac{1}{\rho}\Pi, \tag{3.6}$$

with

$$\Pi = \int p\mathrm{d}t, \tag{3.7}$$

where ϕ' is the potential before impact and ϕ'' is the potential after impact.

Best (1993) applies this formulation of the impact to extend the axisymmetric boundary integral algorithm of Best & Kucera (1992) to compute the evolution of the toroidal phase of a cavity. This method is employed in the present study because it provides an efficient means of following the free surface motion while capturing those features of the impact which determine the surface evolution in the toroidal stage. Since the impact can be considered to be instantaneous on the time scale of the cavity surface motion, the pressure on the cavity surface, $\partial\Omega_c$, which is the pressure, p_c, of the contents of the cavity, is taken as constant. This implies that $\Pi = 0$ for a point on the cavity surface and hence the impact does not change the value of $\phi(\boldsymbol{x})$ for $\boldsymbol{x} \in \partial\Omega_c$.

These considerations allow the formulation of a boundary integral algorithm for the computation of the surface evolution of a cavity from its inception, through expansion and collapse near a rigid boundary and into the toroidal phase following jet impact. The values of ϕ and its normal derivative $\partial\phi/\partial n$ on the boundaries of the liquid domain Ω are related by Green's identity to give

$$\frac{1}{2}\phi(\boldsymbol{x}') = \int_{\partial\Omega}\left(\frac{\partial\phi(\boldsymbol{x})}{\partial n}G(\boldsymbol{x},\boldsymbol{x}') - \phi(\boldsymbol{x})\frac{\partial G(\boldsymbol{x},\boldsymbol{x}')}{\partial n}\right)\mathrm{d}S, \qquad G(\boldsymbol{x},\boldsymbol{x}') = \frac{1}{4\pi|\boldsymbol{x}-\boldsymbol{x}'|} \tag{3.8}$$

(with $\boldsymbol{x}, \boldsymbol{x}' \in \partial\Omega$) for the expansion and collapse of the cavity until just before the moment of jet impact. The impact is assumed to take place at a single point, $\boldsymbol{q}$, in this model (figure 1*b*) which implies that

$$\frac{\partial\phi''}{\partial n} = \frac{\partial\phi'}{\partial n} \tag{3.9}$$

on $\partial\Omega_c$ with $\boldsymbol{q}$ omitted. There is, however, a jump, $\Delta\phi$, in the potential at the point of impact with

$$\Delta\phi = \phi_s(\boldsymbol{q}) - \phi_j(\boldsymbol{q}), \tag{3.10}$$

which defines the induced circulation. The subscripts j, s stand for the liquid jet and opposite cavity surface respectively. In the numerical scheme the surface around the impact is smoothed and a cut C is introduced across the jet, perpendicular to its axis, to define a simply-connected computational domain (see figure 1*c*). The integral formula is now applied to $\partial\Omega_c \cup C$ to compute the evolution of the toroidal cavity,

$$\frac{1}{2}\phi(\boldsymbol{x}') = \int_{\partial\Omega}\left(\frac{\partial\phi(\boldsymbol{x})}{\partial n}G(\boldsymbol{x},\boldsymbol{x}') - \phi(\boldsymbol{x})\frac{\partial G(\boldsymbol{x},\boldsymbol{x}')}{\partial n}\right)\mathrm{d}S - \Delta\phi\int_C \frac{\partial G(\boldsymbol{x},\boldsymbol{x}')}{\partial n_+}\mathrm{d}S, \tag{3.11}$$

using the fact that $\partial G/\partial n_+ = \partial G/\partial n_-$ where $n_\pm$ is the outward normal to respectively the upper and lower surfaces of the cut C. A full account of the method can be found in Best (1993).

The specification of the problem is completed by defining the position of the cavity free surface together with its velocity and potential at some initial time t_0. It is convenient to assume that the cavity is spherical in shape close to the time of its

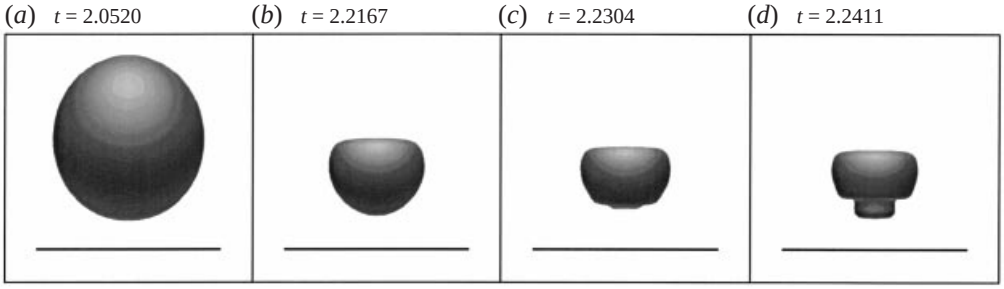

FIGURE 2. Rendered surfaces showing the exterior view of a collapsing cavity for stand-off $\gamma = 1.2$, computed by the numerical method. Times given are non-dimensional.

inception and this agrees with experimental observation. Following Best & Kucera (1992), it is possible to use the Rayleigh–Plesset equation for the oscillation of a spherical cavity in an infinite domain to determine values of α and the initial radius R_0, for a given κ. The boundary integral formulation is then used in conjunction with a second-order, variable-step size, Runge–Kutta method to follow the evolution of the cavity surface from t_0 through expansion and collapse into a toroidal configuration.

4. Numerical results

The results from numerical simulations of the expansion and collapse of a cavity near a plane rigid boundary are presented for a small interval of the stand-off parameter, $0.8 < \gamma < 1.2$. The purpose of the computed examples is to provide a framework showing the range of possible behaviours as a cavity becomes toroidal during the final stage of its collapse. Three typical cases are identified as the depth of the liquid layer between the cavity surface and the rigid boundary is reduced: (i) surface reconnection around the liquid jet; (ii) splash impact at the base of the liquid jet; (iii) thin film splash. As previously mentioned, the term 'splash' refers to the circular liquid film surrounding the liquid jet which is projected out from the quiescent liquid layer by the action of jet impact, but without necessarily breaking into droplets. In case (iii) it is likely that the thin film will break into droplets; however, since the aim here is to provide a qualitative view of the large-scale free surface behaviour, this process is ignored.

The use of smoothing and surface node redistribution in boundary integral calculations for free surface motion is a standard procedure and it is applied here during the toroidal stage to avoid the growth of numerical instabilities. It has the additional effect of reducing the likelihood of surface breaking, but computations carried out with different intervals between smoothing show that the main features of the flows discussed below are retained. This does, though, introduce the assumption that any surface breaking which is smoothed away would not have resulted in the production of droplets or cavities large enough to affect the overall free surface motion. Typically, smoothing is applied every five time steps in the toroidal cavity examples.

The precise contents of the cavities produced in the experiments cannot be determined, but the oscillating behaviour indicates the presence of some non-condensable gas resulting from the initial laser pulse. An arbitrary starting condition at $t = 0$ is chosen for the numerical computations, using the Rayleigh–Plesset equation (Best & Kucera 1992), with the initial non-dimensional radius of the cavity $R_0 = 0.1651$, the initial pressure $\alpha = 100$, the ratio of specific heats $\kappa = 1.4$ and the initial velocity

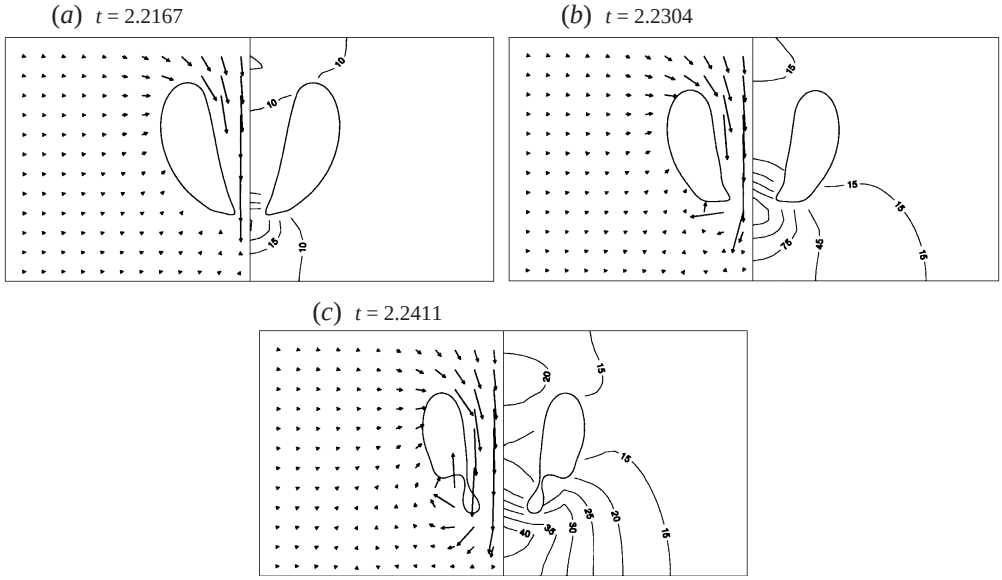

FIGURE 3. Computed surface profiles showing the flow field (left) and pressure contours (right) for $\gamma = 1.2$. Times and pressures are non-dimensional.

on the free surface set to zero. Other starting conditions were investigated with a smaller proportion of non-condensable contents giving a shorter period of oscillation, but with the main features of the surface motion being retained. The numerical examples are therefore not matched precisely to the time of the cavity period in the experiments. However, the computed time interval covering the jet impact and splashing events is found to agree closely with the experiments. Where times are given in the figures showing the computed examples, a non-dimensional time interval of $\Delta t^* = 0.02$ corresponds to $\Delta t \approx 2.6$ μs in the experiments, where the bubble maximum radius is 1.3 mm and the density of water is taken as 999.7 kg m^{-3}. The pressure scale is $\Delta p \approx 10^5$ Pa and the pressure contours in the computed figures are given in this scale, so that a non-dimensional pressure of 100 corresponds to 10 MPa in the experiments. However, the pressure records from the experiments are complicated by the presence of short-duration acoustic transients which are left out of consideration in the present model. The three typical cases are described below.

4.1. *Surface reconnection around the liquid jet*

For a stand-off of $\gamma = 1.2$ (figures 2 and 3), the liquid layer between the cavity surface and the rigid boundary has a depth of 0.2 at maximum expansion. During the collapse, the depth of the liquid separating the cavity from the boundary remains at about 0.2 through to jet impact (figure 2*b*). Following a lateral contraction of the cavity (figure 2*a*) the part of the surface furthest from the boundary flattens leading to the formation of a high-speed jet which threads the cavity. The jet impact causes an extension of the cavity as the liquid of the jet is forced radially outwards from its axis under the influence of the region of high pressure which develops at the impact site. This effect, combined with the circulation induced by the impact and the continued contraction of the cavity, gives the appearance of a rapid motion of the surface of the main part of the cavity away from the boundary, leaving a stalk-like protrusion as shown in figure 2(*d*). The development of a fully-formed splash is prevented by

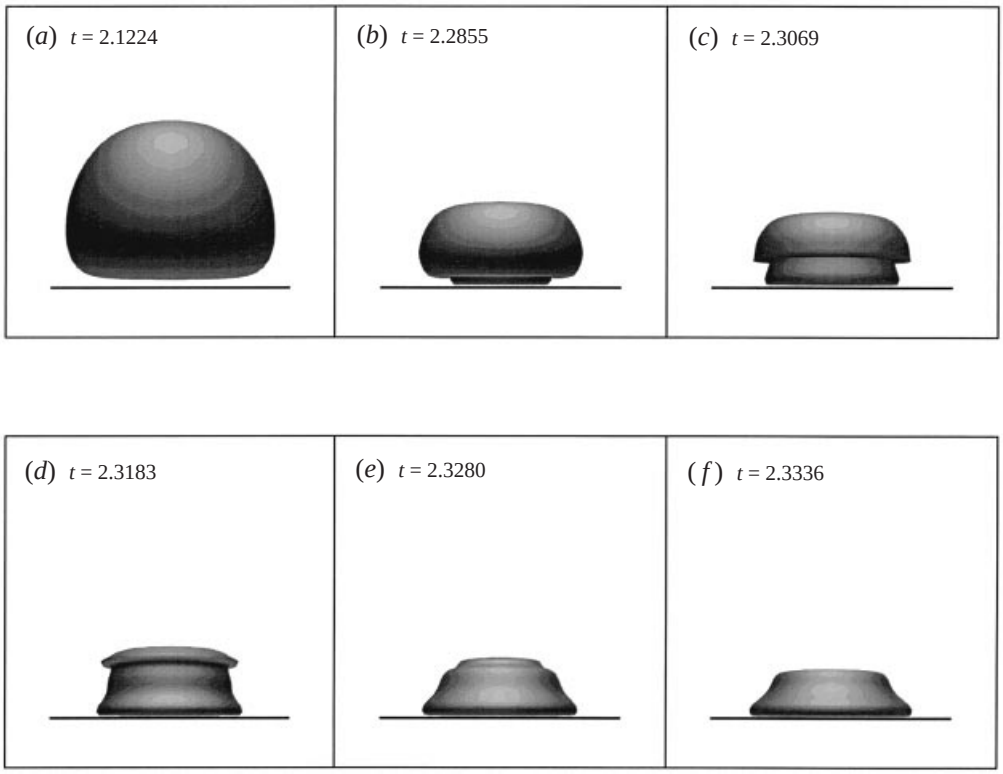

FIGURE 4. Rendered surfaces showing the exterior view of a collapsing cavity for stand-off $\gamma = 0.92$, computed by the numerical method. Splash impact occurs between frames (*d*) and (*e*). Times given are non-dimensional.

reconnection of the liquid surface surrounding the lower part of the jet with that of the jet, resulting in the separation of a portion of the cavity contents from the main volume. Since the computation is an idealization, there could be further breakup of the vapour and gas in the region of the jet tip to form many small cavities. The main part of the cavity remains to re-expand from minimum volume, but the present numerical algorithm does not allow the motion to be tracked further in time.

It can be seen from figure 3 that the hydrodynamic pressures generated by the jet impact are localized around the jet tip and the pressures registered on the boundary are much less than the peak pressures in the liquid. Similar cases are reported by Ohl *et al.* (1995). For $\gamma = 2.0$, two shock waves are emitted by the cavity at first collapse, the first of these being centred on the region of jet impact. Our investigation does not cover this value of γ and shock waves are not visible in the frames presented in Ohl *et al.* (1995) for jet impact at first collapse when $\gamma = 1.2$.

4.2. *Splash impact at the base of the liquid jet*

The numerical results for $\gamma = 0.92$ illustrate the effect of the boundary on the generation of a splash (figures 4 and 5). The jet impact is onto a thin liquid layer and the proximity of the boundary produces a radial flow outwards from the jet axis. This radial flow meets the inward motion of liquid induced by the collapsing cavity and a splash is projected from the thin liquid layer on the boundary surrounding the jet, moving in a direction opposite to that of the jet. Viewed externally, the cavity assumes

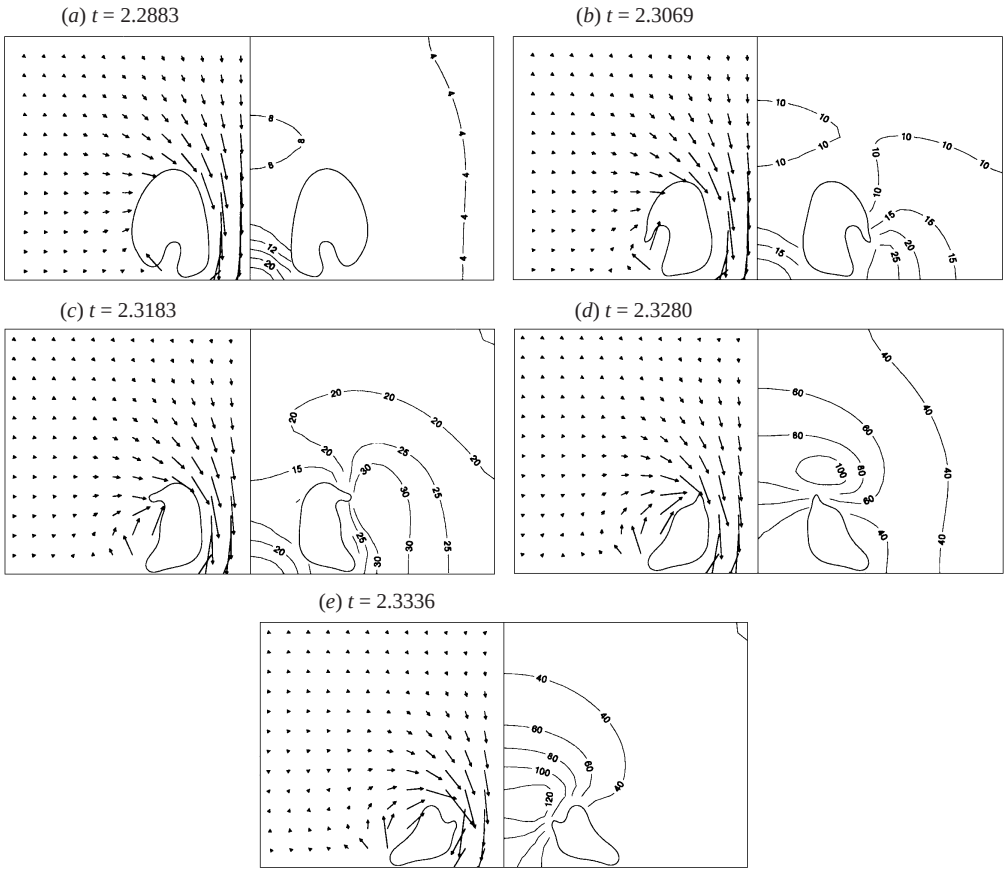

FIGURE 5. Computed surface profiles showing the flow field (left) and pressure contours (right) for $\gamma = 0.92$. Times and pressures are non-dimensional.

a mushroom-like shape as the splash rises around the jet (figure 4*c*). The outward radial flow along the boundary causes the base of this mushroom shape, which is close to the boundary, to spread. In the case of liquid impact onto a plane liquid surface, the splash would propagate radially with gravity effects becoming evident. In the setting of the surface of a cavity, the splash is constrained to propagate around the closed surface and is thus focused towards the base of the jet. The speed of the upward splash, relative to the surface of the cavity furthest from the boundary, is approximately the same as the initial jet speed. There is thus a violent impact when the splash meets the upper cavity surface on a ring around the jet base. The present computations indicate that pressures generated by the splash impact are as much as ten times greater than those at jet impact. This high-pressure region is not in contact with the boundary, but results in higher pressures than those at jet impact being registered there, in an annular region around the base of the cavity (figure 5*c*, *d*).

As in the previous case the numerical results represent an idealized regime, with surface smoothness being maintained even though there is the likelihood that small cavities will be formed by surface breaking during the splash impact. Compressible effects of the splash interaction are ignored by the numerical model. The ring of high pressure now drives the flow through the centre of the torus and forces the cavity towards the boundary causing it to spread in the radial direction. It is at this time

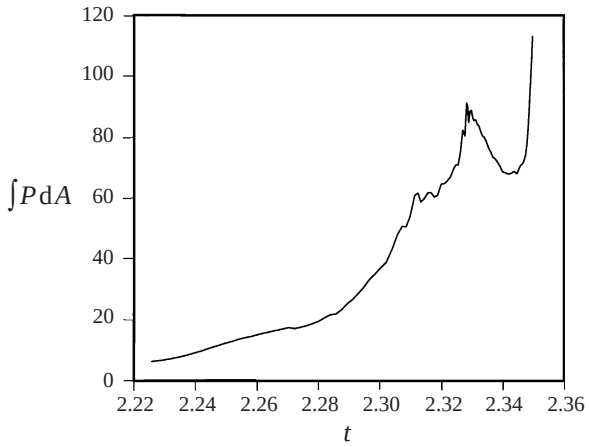

FIGURE 6. Computed pressure loading ($\int P\mathrm{d}A$) for $\gamma = 0.92$ on the rigid boundary over a circular region of radius 1, centred on the axis of symmetry. Time and loading scales are non-dimensional.

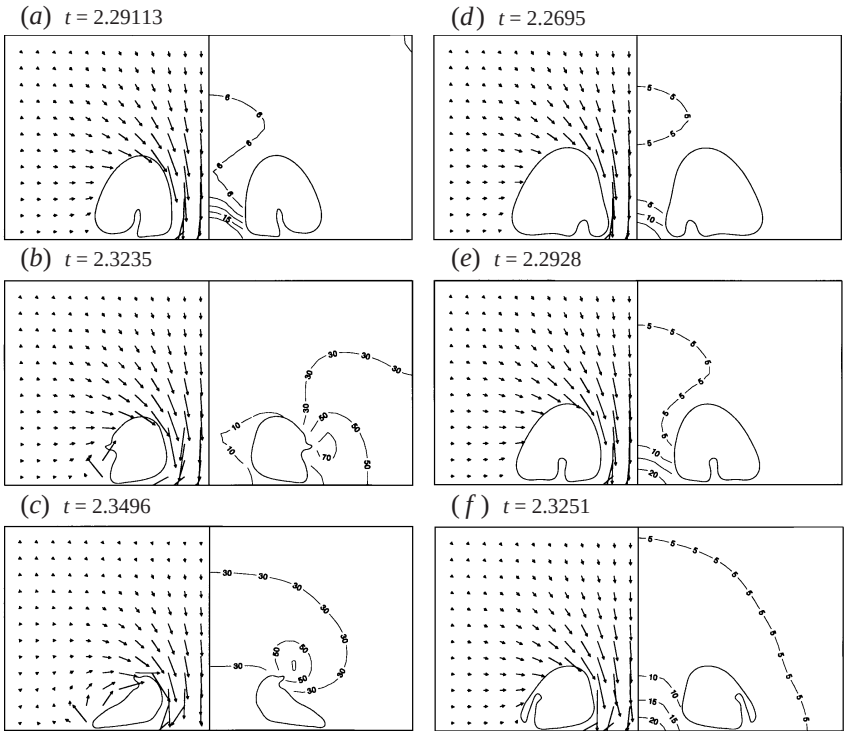

FIGURE 7. Computed thin film splash, surface profiles: $\gamma = 0.85$ (*a*)–(*c*) leading to splash impact at base of jet, $\gamma = 0.81$ (*d*)–(*f*) leading to splash impact at sides of cavity. Times and pressures are non-dimensional.

that the cavity reaches minimum volume and starts to re-expand which increases the loading on the boundary (figures 4*f* and 5*e*). Figure 6 shows the pressure loading on the boundary calculated by integrating the pressure over a disc with radius equal to that of the cavity at maximum expansion. (In the experiments, the transducer size is 1.15 times the maximum cavity radius.) The curve starts from the formation of

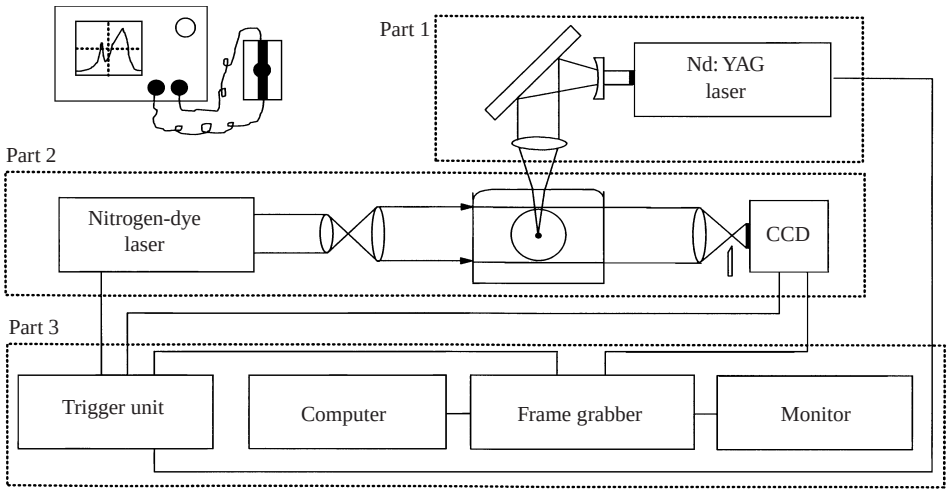

FIGURE 8. Experimental set-up.

the toroidal cavity at jet impact and the peak at $t \approx 2.33$ corresponds to the splash impact. The sharp rise in the loading following this peak is due to the accelerating flow through the torus coinciding with the rebound of the cavity. Beyond this stage the computation is likely to be unreliable as the cavity surface spreads along the boundary. A time interval of 0.12 encompasses the events from jet impact through to the second pressure peak and corresponds to a time of 16 μs for a 1.3 mm cavity under the conditions of the experiments described below.

4.3. *Thin film splash*

The computation for the case $\gamma = 0.85$ shows that, as the point of cavity inception is moved closer to the boundary, the liquid film between the jet tip and the rigid boundary at the time of impact becomes thinner and the diameter of the base of the cavity close to the wall increases. The jet impact gives rise to a thin film splash (figure 7*a–c*) which propagates outwards on the radial flow due to the jet and travels around the cavity surface to produce an impact at the base of the jet as in the preceding case. However, the impact is a smaller event corresponding to the smaller mass of liquid displaced into the splash. It is possible that the splash film would breakup into droplets to some extent, but this is not allowed for in the present numerical model. Computations for $\gamma = 0.81$ show that the rim of the thin film splash can meet the cavity surface at the sides while it is still propagating outward on the radial flow along the boundary. This splash impact leads to the entrapment of a portion of the cavity contents and a breakup of the original cavity (figure 7*d–e*). The computation cannot be continued beyond this time.

5. Experimental method

The optical apparatus used to carry out the high-speed study of the laser-generated cavities is divided into three parts as shown in figure 8.

The first part comprises a Q-switched Nd:YAG laser which emits a coherent beam of light at a wavelength of $\lambda = 1064$ nm with an output pulse energy of about 100 mJ and a pulse width of $\Delta\tau = 30$ ns. The laser radiation is first expanded by a biconcave lens and then focused by a 25 mm focal length plano convex lens to produce a cone

angle of 9° and a final beam waist in the water of about 10 μm. The plasma is formed during the 20 ns pulse of the Nd:YAG laser and over this time interval the plasma grows along the laser beam axis. The vapour bubble then expands around the plasma and soon becomes spherical so that the bubble no longer 'remembers' the formation condition very early in its life.

The second part of the experimental set-up consists of the high-speed image recording system. The ultra fast light source to illuminate the high-speed event in the water tank is a dye laser which emits a green coherent light beam with a coherence length of 20 μm at a wavelength of $\lambda = 512$ nm. The green coumarin 500 dye was excited by a pulsed nitrogen gas laser ($\lambda = 337$ nm). The beam of the dye laser with an energy of about 15 μJ and a pulse duration of 500 ps is spatially filtered by a ×40 microscope objective and a 25 μm pinhole. This removes the slightly varying parts of the laser beam as well as any scattered light. Leaving the spatial filter, the laser beam passes through a 50 mm focal length camera lens so that a parallel beam of light illuminates the cavitation event. The event is focused on the sensitive area of a CCD camera by a 135 mm focal length camera lens. Between the camera lens and the CCD camera a knife used as a schlieren edge is positioned half-way in the waist of the beam. Therefore light rays which are deviated by the refractive index changes in the water associated with the high-speed event are cut off by the knife edge producing a schlieren image on the sensitive area of the CCD camera. The test area is a water tank with the dimensions $5 \times 5 \times 5$ cm^3 filled to the brim with deionized water so as to form a positive meniscus which can be seen at the upper edge of the tank.

The third part of the experimental arrangement comprises a personal computer, a frame grabber system and a CCD camera. The trigger ensures accurate synchronization between the Nd:YAG laser and the dye laser. A suitable delay time between firing the two lasers is chosen manually and was varied between 0.6 μs (which is the time delay between the emission of the nitrogen laser and the occurrence of the dye illumination) and 450 μs until a series of images of the region of interest has been obtained. An analogue video signal from the CCD camera is digitized and held in the frame store with a 512×512 pixel array and 64 grey levels. This signal is then passed to the computer for permanent storage and can be displayed on a monitor. Printouts were obtained on a thermal printer. The recorded images show a spatial resolution of about 28 μm which originates from the 7 mm wide horizontal field of the CCD camera.

To measure the pressure development of a collapsing cavity in front of the boundary a thin film transducer is stuck to a PMMA block. The active material of the keyhole shaped transducer has a diameter of 3 mm and is made from polyvinylidene fluoride (pvdf). This is covered by two Silver Ink electrodes and has a total thickness of 52 μm. The speed of sound is 2.2 mm μs^{-1} giving a transit time of 24 ns, which is therefore the rise time of the voltage signal for a step pressure pulse resulting from a plane wave at normal incidence on the transducer. However, in the present application the pressure impulse is best described by a spherical wave where the relatively large area of the transducer at small stand-off distances means that the pressure signal is a convolution of the two functions: spherical wave and rise.

Previous work using high-resolution Mach–Zehnder interferometry of laser-generated acoustic transients in unbounded liquids has given the spatial and temporal profile of the initial and subsequent acoustic transients (Ward & Emmony 1991). The pressure profiles measured by the two techniques are found to be identical. The initial breakdown transient has the shortest rise time and is illustrated in Shaw *et al.* (1996). More recently it has been shown that these thin piezoelectric transducers may be

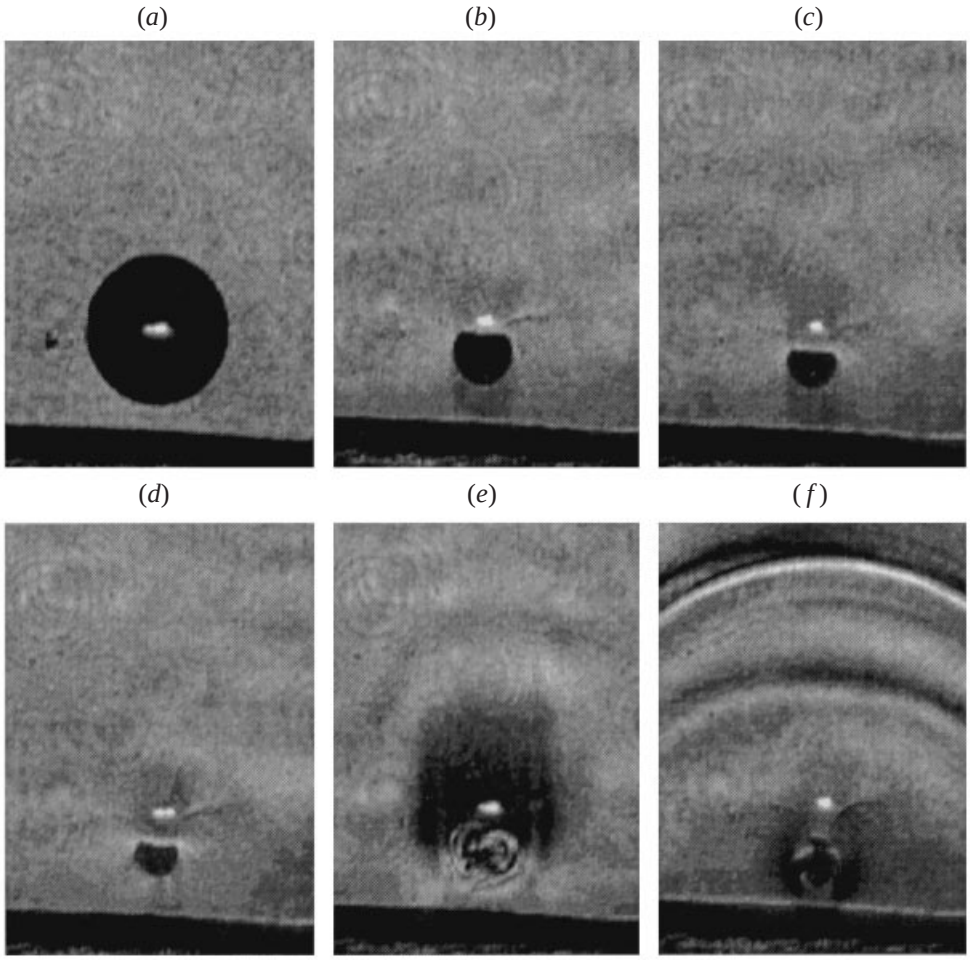

FIGURE 9. Schlieren images of collapse of laser-generated cavity, $\gamma = 1.2$.

used to measure the waveform. The transducer has been calibrated against the optical experimental results and there is also good agreement with the calculated sensitivity provided by the manufacturer of the pvdf film (Kynar). The peak pressure at initial breakdown was 40 MPa and at the first collapse of a 1.3 mm radius cavity with $\gamma = 0.92$ it was 11 MPa (figure 12).

The output pressure signal of the transducer is displayed on a digital storage oscilloscope. Even though every single laser shot generates a different cavitation event, the experiment is very reproducible and hence the schlieren images obtained can be regarded as a sequence. Although each cavity undergoes several oscillations, attention is here focused on the first collapse and so transducer plots in most cases were not continued as far as the second collapse.

6. Experimental results

6.1. $\gamma \approx 1.2$

The schlieren images shown in figure 9(*a–c*) are very similar to the numerical simulation of figure 2(*a–c*). The flattening of that part of the cavity surface furthest from

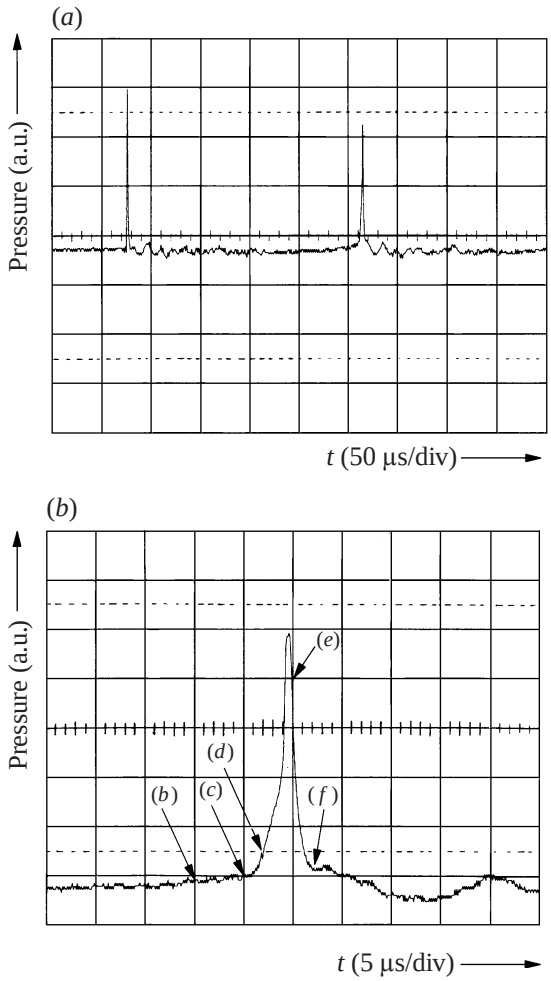

FIGURE 10. Pressure loading (arbitrary units) on the boundary for $\gamma = 1.2$: (*a*) showing cavity inception (first peak) and first collapse (second peak); (*b*) at first collapse indicating times of frames in figure 9.

the boundary can be interpreted as due to the formation of the jet which threads the cavity. Shortly after the jet impact there is a noticeable contraction of the cavity away from the boundary, which is in agreement with the numerical prediction of reconnection of the free surface around the jet leading to entrainment of some of the cavity contents. The protrusion below the cavity shown in figure 2(*d*) is not visible in the experimental images; however, the photographs of Tomita & Shima (1986) for $\gamma = 1.23$ and $\gamma = 1.10$ show that there is likely to be some variation in the breakup of the cavity around the jet tip. The numerical simulation gives a general indication of this behaviour. Figure 10(*a*) shows the pressure record for a transducer of radius 1.5 mm where the maximum cavity radius is 1.3 mm. The first peak corresponds to the initial laser breakdown in water which generates the cavity, while the second peak is due to effects around the first minimum volume of the cavity. The pressure induced on the wall for this case shows a short-duration pressure pulse, and shock waves are evident in figure 9(*e*,*f*). Comparison with the surface shapes of figure 2 suggests that the jet impact in the experiment is close to the time of figure 9(*b*) and certainly before

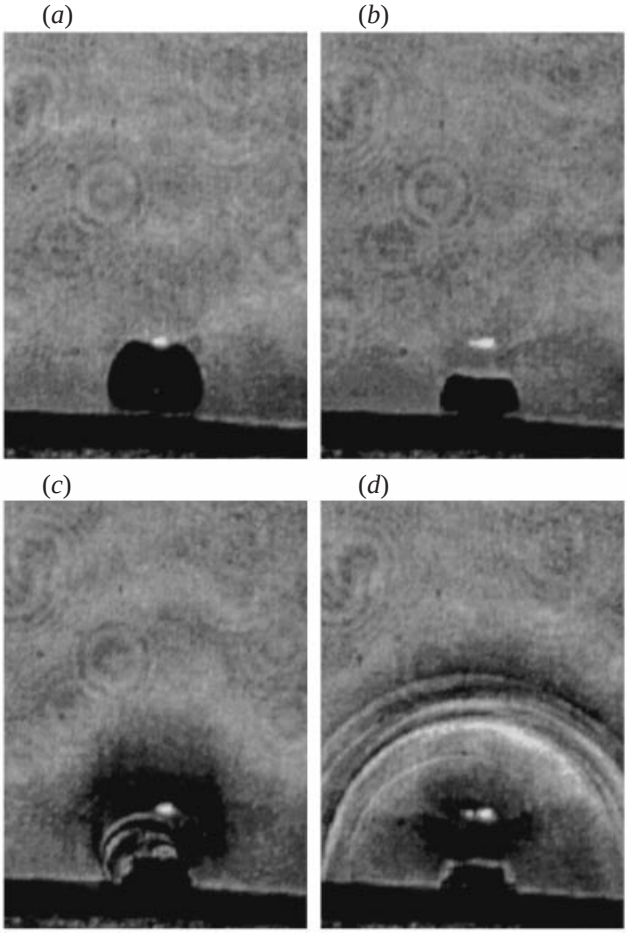

FIGURE 11. Schlieren images of collapse of laser-generated cavity, $\gamma = 0.92$.

that of figure 9(*c*). The times of these frames are indicated in figure 10(*b*) and it is clear that the dominant pressure loading occurs about 5 μs after jet impact mainly due to the shock effects as the cavity rebounds.

6.2. $\gamma \approx 0.92$

The schlieren images from the experiment in this case can be interpreted in terms of the splash effect described in §4.2. The surface shapes of figure 11 match closely those of figure 4, with 11(*b*) showing the toroidal cavity shortly after jet impact as the splash begins to rise away from the boundary creating a mushroom-like shape. Figure 11(*c*) shows shock waves being emitted as the splash reaches the top of the cavity and the cavity moves towards the boundary while spreading outwards (figure 11*d*). The corresponding pressure loading on the boundary is illustrated in figure 12, where (*a*) shows the initial laser pulse followed by the first collapse, while the third peak is due to the second collapse. The first collapse, involving the splash effect, gives lower pressures than at the second collapse and this agrees with the results for $0.7 < \gamma < 1.0$ reported earlier by Tomita & Shima (1986). It should also be noted that the splashing phenomenon is associated with a peak of longer duration than those due to shocks. The positions of the frames of figure 11 are marked in figure 12(*b*). It can be seen that

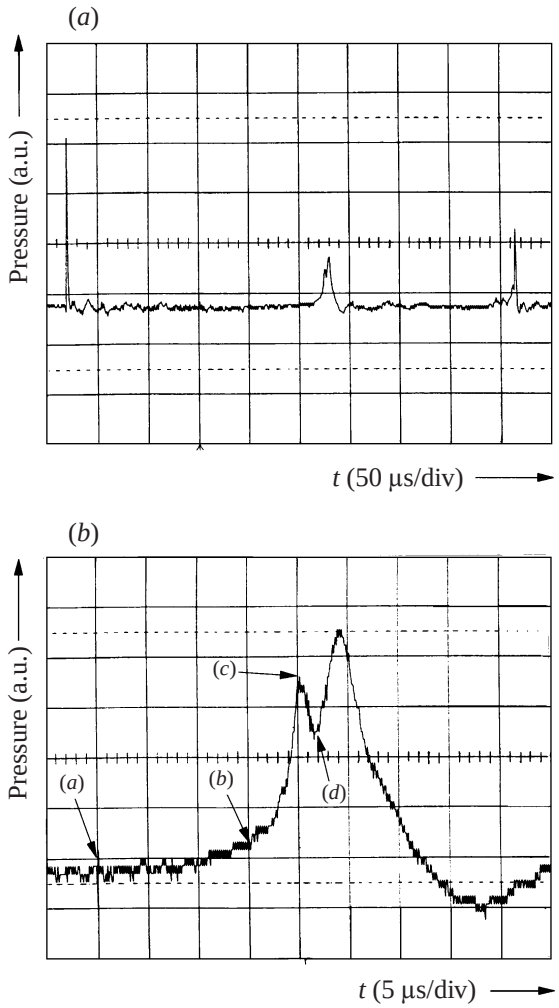

FIGURE 12. Pressure loading (arbitrary units) on the boundary for $\gamma = 0.92$: (*a*) showing cavity inception (first peak), first collapse (second peak) and second collapse (third peak); (*b*) double peak at first collapse with times of frames in figure 11 indicated.

for a transducer of radius approximately that of the cavity at maximum expansion, the jet impact does not register as a significant event. The double-peaked structure that occurs in the pressure profile can be interpreted in the light of the numerical results. The first maximum in figure 12(*b*) coincides with the splash impact at the base of the liquid jet (the top of the bubble in figure 11) and this event is associated with the emission of shock waves. The second maximum corresponds to the subsequent acceleration of the flow through the torus and the start of the re-expansion of the cavity. The time interval of 16 μs predicted by the numerical method can be seen to agree with the timing of these events in the experiment from jet impact (figure 11 between frames *a* and *b*) to the second pressure peak.

6.3. $\gamma \approx 0.81$

As the stand-off distance is reduced, the radius of the base of the cavity adjacent to the boundary increases and the numerical simulation suggests that in this case a thin

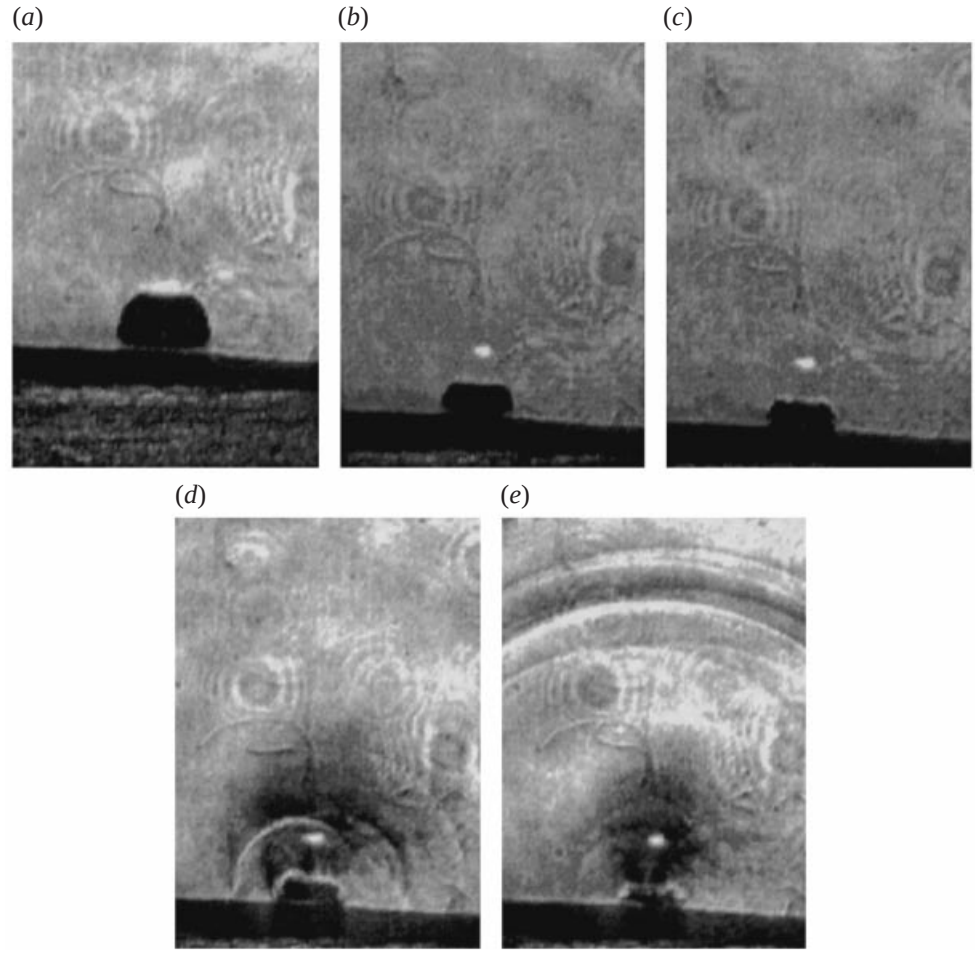

FIGURE 13. Schlieren images of collapse of laser-generated cavity, $\gamma = 0.81$.

film splash propagates radially outward from the jet axis after impact. It can be seen from figure 13(*c*, *d*) and figure 14(*b*) that the first maximum of the double-peaked pressure profile produced by the collapse corresponds to the emission of shock waves. The breaking of the cavity surface evident in figure 13(*e*) and the cavity shapes leading up to this are consistent with a splash impact around the sides of the cavity as in figure 7(*d–f*) which occurs before the splash disturbance can reach the top of the cavity. Figure 14(*a*) indicates that the cavity re-forms during the second expansion and produces a short-duration shock-pressure at the second rebound.

7. Conclusions

The present investigation of collapsing cavities near a rigid boundary for the stand-off parameter in the interval $0.8 < \gamma < 1.2$ reveals complex interactions involving jet impact and splashing. As the cavity inception point is brought closer to the boundary, there is a decrease in the peak pressures recorded, contrary to expectation, but in agreement with the earlier results of Tomita & Shima (1986). However, while the

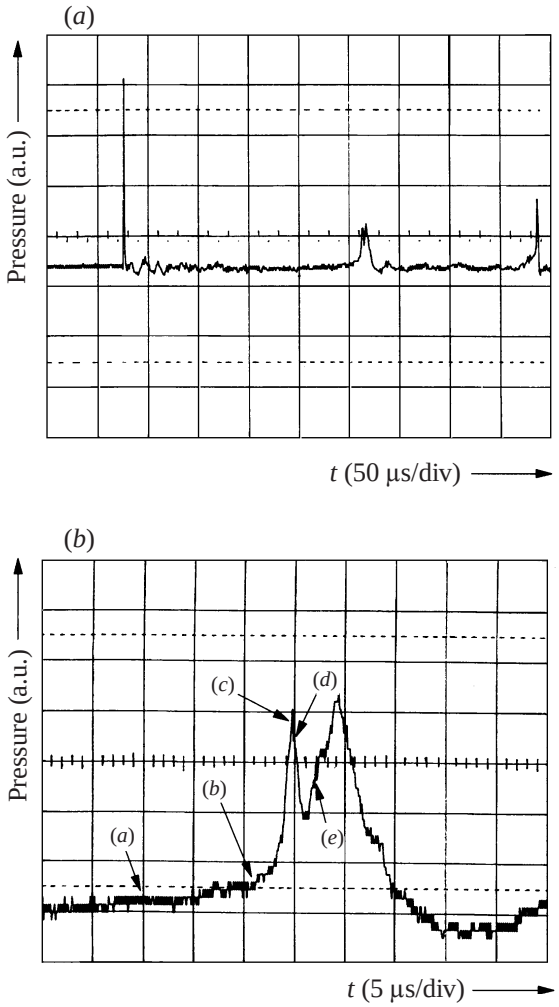

FIGURE 14. Pressure loading (arbitrary units) on the boundary for $\gamma = 0.81$: (*a*) showing cavity inception (first peak), first collapse (second peak) and second collapse (third peak); (*b*) double peak at first collapse with times of frames in figure 13 indicated.

short-lived shock pressures become less important, large hydrodynamic pressures of longer duration are produced by the flow around the toroidal cavity as it rebounds.

A typical case for the splash interaction (e.g. for $\gamma = 0.92$) shows the following sequence of events during the final stage of collapse. The impact of the liquid jet which threads the cavity occurs on a thin layer of liquid separating the cavity from the boundary and results in the formation of a splash as the radial flow outward along the boundary from the jet axis meets the inflow due to the contracting cavity. This splash is constrained to follow the cavity free surface and is thus focused at the base of the still-flowing liquid jet (at the top of the cavity when viewed with the boundary below). There is a violent splash impact where the relative velocity of the splash rim is approximately the same as that of the jet just before impact (100 m s^{-1} in the present experiments). Shock waves are emitted at this impact and the cavity is forced towards the boundary by the resulting high-pressure region. This coincides with the cavity reaching minimum volume and beginning to rebound leading to an

acceleration of the flow through the centre of the toroidal cavity. The pressure record from a transducer of radius approximately that of the maximum expansion of the cavity shows two peaks at this collapse. The first maximum is identified with the shock waves resulting from splash impact and is followed by a second peak which is due to the resulting flow through the torus. The jet impact does not register as a significant event on this pressure record.

When the cavity is further from the boundary (for $\gamma = 1.2$) there is reconnection of the cavity surface around the jet, leading to entrainment of some of the cavity contents. This is observed as a sudden contraction away from the boundary of the main cavity surface. As the cavity inception point is brought closer to the boundary, the radius of the base of the cavity increases and the layer of liquid between the cavity and the boundary becomes thinner, giving rise to a thin film splash propagating along the boundary on the radial flow after jet impact. There is a splash impact around the sides of the cavity leading to breakup of its surface ($\gamma = 0.81$).

Further investigations are planned to determine the behaviour of collapsing cavities for $\gamma < 0.8$. In addition, computations indicate the possibility of other splash–cavity interactions depending on the timing of the jet impact in relation to the cavity rebound.

Funding for this work from the EPSRC and the DERA, Fort Halstead, is gratefully acknowledged.

REFERENCES

Batchelor, G. K. 1967 *An Introduction to Fluid Dynamics*. Cambridge University Press.

Benjamin, T. B. & Ellis, A. T. 1966 The collapse of cavitation bubbles and the pressures thereby produced against solid boundaries. *Phil. Trans. R. Soc. Lond.* A **260**, 221–240.

Best, J. P. 1993 The formation of toroidal bubbles upon the collapse of transient cavities. *J. Fluid Mech.* **251**, 79–107.

Best, J. P. & Kucera, A. 1992 A numerical investigation of non-spherical rebounding bubbles. *J. Fluid Mech.* **245**, 137–154.

Bourne, N. K., Obara, T. & Field, J. E. 1996 The impact and penetration of a water surface by a liquid jet. *Proc. R. Soc. Lond.* A **452**, 1497–1502.

Bourne, N. K., Obara, T. & Field, J. E. 1997 High-speed photography and stress gauge studies of jet impact upon surfaces. *Phil. Trans. R. Soc. Lond.* A **355**, 607–623.

Bowden, F. P. & Brunton, J. H. 1961 The deformation of solids by liquid impact at supersonic speeds. *Proc. R. Soc. Lond.* A **263**, 433–450.

Cole, R. H. 1948 *Underwater Explosions*. Princeton University Press.

Cresswell, R. W. & Morton, B. R. 1995 Drop-formed vortex rings – the generation of vorticity. *Phys. Fluids* **7**, 1363–1370.

Fujikawa, S. & Akamatsu, T. 1980 Effects of the non-equilibrium condensation of vapour on the pressure wave produced by the collapse of a bubble in a liquid. *J. Fluid Mech.* **97**, 481–512.

Gilbarg, D. & Anderson, R. A. 1948 Influence of atmospheric pressure on the phenomena accompanying the entry of spheres into water. *J. Appl. Phys.* **19**, 127–139.

Guo, Y. P. & Ffowcs Williams, J. E. 1991 A theoretical study on drop impact sound and rain noise. *J. Fluid Mech.* **227**, 345–355.

Hand, R. J., Field, J. E. & Townsend D. 1991 The use of liquid jets to simulate angled drop impact. *J. Appl. Phys.* **70**, 7111–7118.

Howison, S. D., Ockendon, J. R. & Wilson, S. K. 1991 Incompressible water-entry problems at small deadrise angles. *J. Fluid Mech.* **222**, 215–230.

Johnson, W. & Vickers, G. W. 1973 Transient stress distribution caused by water-jet impact. *J. Mech. Engng. Sci.* **15**, 302–310.

Korobkin, A. A. 1997 Asymptotic theory of liquid-solid impact. *Phil. Trans. R. Soc. Lond.* A **355**, 507–522.

LAUTERBORN, W. 1974 Kavitation durch laserlicht. *Acustica* **31**, 51–78.

LESSER, M. B. 1981 Analytic solutions of liquid-drop impact problems. *Proc. R. Soc. Lond.* A **377**, 289–308.

OĞUZ, H. N. & PROSPERETTI, A. 1989 Surface-tension effects in the contact of liquid surfaces. *J. Fluid Mech.* **203**, 149–171.

OĞUZ, H. N., PROSPERETTI, A. & KOLAINI, A. R. 1995 Air entrapment by a falling water mass. *J. Fluid Mech.* **294**, 181–207.

OHL, C. D., PHILIPP, A. & LAUTERBORN, W. 1995 Cavitation bubble collapse studied at 20 million frames per second. *Ann. Physik* **4**, 26–34.

PEREGRINE, D. H. & KALLIADASIS, S. 1996 Filling flows, cliff erosion and cleaning flows. *J. Fluid Mech.* **310**, 365–374.

PHILIPP, A. & LAUTERBORN, W. 1997 Damage of solid boundaries by single laser-produced cavitation bubbles. *Acustica* **83**, 223–227.

PHILIPP, A. & LAUTERBORN, W. 1998 Cavitation erosion by single laser-produced bubbles. *J. Fluid Mech.* **361**, 75–116.

RAYLEIGH, LORD 1917 On the pressure developed in a liquid during the collapse of a spherical void. *Phil. Mag.* **34**, 94–98.

REIN, M. 1996 The transitional regime between coalescing and splashing drops. *J. Fluid Mech.* **306**, 145–165.

ROGERS, J. C. W. & SZYMCZAK, W. G. 1997 Computations of violent surface motions: comparisons with theory and experiment. *Phil. Trans. R. Soc. Lond.* A **355**, 649–663.

SHAW, S. J., JIN, Y. H., SCHIFFERS, W. P. & EMMONY, D. C. 1996 The interaction of a single laser generated cavity in water with a solid surface. *J. Acoust. Soc. Am.* **99**, 2811–2824.

TOMITA, Y. & SHIMA, A. 1986 Mechanisms of impulsive pressure generation and damage pit formation by bubble collapse. *J. Fluid Mech.* **169**, 535–564.

VOGEL, A. & BUSCH, S. 1994 Time-resolved measurements of shock-wave emission and cavitation-bubble generation in intraocular laser surgery with ps- and ns- pulses. In *Bubble Dynamics and Interface Phenomena*, (ed. J. R. Blake, J. M. Boulton-Stone, & N. H. Thomas), pp.105–117. Kluwer.

VOGEL, A. & LAUTERBORN, W. 1988 Acoustic transient generation by laser-produced cavitation bubbles near solid boundaries. *J. Acoust. Soc. Am.* **84**, 719–731.

VOGEL, A., LAUTERBORN, W. & TIMM, R. 1989 Optical and acoustic investigations of the dynamics of laser-produced cavitation bubbles near a solid boundary. *J. Fluid Mech.* **206**, 299–338.

WARD, B. & EMMONY, D. C. 1991 Interferometric studies of the pressures developed in a liquid during infrared-laser-induced cavitation-bubble oscillation. *Infrared Phys.* **32**, 489–515.

YARIN, A. L. & WEISS, D. A. 1995 Impact of drops on solid surfaces: self-similar capillary waves, and splashing as a new type of kinematic discontinuity. *J. Fluid Mech.* **283**, 141–173.

ZHANG, S., DUNCAN, J. H. & CHAHINE G. L. 1993 The final stage of the collapse of a cavitation bubble near a rigid wall. *J. Fluid Mech.* **257**, 147–181.